DESCRIBING FUNCTION PROPERTIES OF A MAGNETIC PULSE-WIDTH MODULATOR

R. D. Middlebrook
California Institute of Technology
Pasadena, California 91109

ABSTRACT

An analysis is presented for the transfer functions of a particular pulse-width modulator and power switch subsystem that has been widely used in practical switching-mode d-c regulator systems. The switch and filter are in a "buck" configuration, and the switch is driven by a constant-frequency variable duty-ratio push-pull magnetic modulator employing square-loop cores. The two transfer functions considered are that with modulator control signal as input and that with line voltage as input. For a-c signals, the corresponding describing functions (DF) are derived. It is shown that current-source drive to the modulator extends the control DF frequency response over that with voltage drive, and that complete cancellation of the effects of line variations can be obtained at d-c but not for a-c. Experimental confirmation of the analytical results for the control DF are presented.

1. INTRODUCTION

In switching mode d-c regulators and amplifiers, a control signal modulates the duty ratio of a switch associated with a line voltage and a low-pass filter. This subsystem of modulator and power stage is usually part of an overall feedback loop, as shown schematically in Fig. 1, whose regulation and stability depend upon two properties of the subsystem: the control signal to output voltage transfer function and the line voltage to output voltage transfer function. The d-c transfer functions are easily understood and analyzed, but analysis of the a-c transfer functions presents considerable difficulties because, since the subsystem effectively contains an A-to-D and a D-to-A converter, it is inherently nonlinear. For many practical systems the problem of absence of quantitative understanding of the a-c transfer functions is merely avoided by introduction of a sufficiently low-frequency dominant pole in the overall feedback loop to ensure stability. The result is poorer system performance than might otherwise be obtained.

This paper presents an analysis for the transfer functions of a particular modulator and power stage subsystem. However, before introduction of the particular subsystem, a more detailed discussion of the nature of the generalized subsystem of Fig. 1 will be given in order to establish the specific definitions of the analysis goals.

If the line voltage $v_\ell(t)$ has a constant d-c value V_ℓ and the control signal is a constant d-c voltage V_c, the modulator delivers a digital switch drive that turns the switch on and off with a constant duty ratio D and a constant repetition, or switching, frequency f_s. The output voltage $v_o(t)$ contains a constant d-c component V_o, and also harmonics of the switching frequency f_s.

If again the line voltage is constant at V_ℓ but the control signal consists of a d-c voltage V_c plus a sinusoidal component $\hat{v}_c$ at frequency f, where $\hat{v}_c$ is expressed in phasor form, the duty ratio and perhaps also the switching frequency change at the frequency f, and the resulting output voltage contains, in addition to the d-c component V_o and harmonics of f_s, a phasor component $\hat{v}_o$ at the control frequency f and components at higher harmonics of f and also sidebands at sum and difference frequencies of the harmonics of f_s and f. A statement of the complete control signal to output voltage transfer function is therefore very complicated, and any attempt to determine the stability of the overall feedback loop is even more so. What one would like is to ignore all components of the output voltage other than those at d-c and the control frequency; the remaining components, at least for control frequencies much lower than the switching frequency are in fact purposely made small by inclusion of the low-pass filter. The relation between a sinusoidal input signal and the resulting output voltage component at the same frequency $\omega = 2\pi f$, where both are expressed in phasor form, is known as the describing function, so the control signal to output voltage describing function F_c is defined as

$$F_c(j\omega) = \frac{\hat{v}_o}{\hat{v}_c} \qquad (1)$$

under conditions of constant line voltage $v_\ell(t) = V_\ell$.

A similar discussion may be made for the condition in which the control signal is constant but the line voltage consists of a d-c voltage V_ℓ plus a sinusoidal component $\hat{v}_\ell$ in phasor form at frequency $\omega = 2\pi f$. Output voltage components at frequencies other than f are ignored, and the line voltage to output voltage describing function is defined as

$$F_\ell(j\omega) = \frac{\hat{v}_o}{\hat{v}_\ell} \qquad (2)$$

under conditions of constant control signal $v_c(t) = V_c$.

It may be noted that neither describing function may be linear in that its value may depend upon the amplitude of the relevant sinusoidal input signal. It is therefore convenient to define the linearized describing function as the limit of the describing function as the amplitude of the input signal becomes vanishingly small. The usefulness of the linearized describing functions is that the actual nonlinear subsystem of Fig. 1 can be approximately modeled by a "black box" characterized by linear transfer functions. As a result, the large body of linear system theory can be invoked to investigate the performance and stability of the complete regulator or amplifier. It must be remembered, however, that because of the approximations implicit in the linearized describing function representation, a stability criterion, as obtained for example from a Nyquist plot, constitutes a necessary but perhaps not sufficient condition for stability.

There are many ways in which the power stage and modulator of Fig. 1 can be implemented in practical systems. For example, the power stage may be implemented by a switch and LC filter in the familiar buck, boost, or buck-boost configuration. The modulator of necessity samples the control signal to produce the digital switch drive; the sampling may be uniform, natural, or any of various integrating types, and the resulting digital switch drive may be constant on-time, constant off-time, or constant on-plus-off time (constant, or clocked, frequency).

The purpose of this paper is to present analytical expressions for the linearized control signal to output voltage and line voltage to output voltage describing functions for a particular modulator and power stage subsystem that has been widely used in practical switching-mode d-c regulator systems.

2. QUALITATIVE OPERATION OF A MAGNETIC MODULATOR AND POWER STAGE

The particular implementation of the modulator and power stage subsystem to be considered is shown in Fig. 2, in which the waveforms are those for steady-state, or d-c, operation in which the line voltage is constant at V_ℓ and the control signal is a constant voltage V_c. For analysis purposes all diodes and the power switch are assumed ideal. The switch and filter are in a buck configuration, and the switch is driven by a constant frequency variable duty-ratio push-pull magnetic modulator employing square-loop cores. The control windings are shown driven by a Thevenin equivalent source voltage V_c and resistance R_c, and the gate windings are driven from a square-wave clock oscillator of frequency $f_s/2$. The principle of operation is well-known and need be only briefly summarized. The volt-seconds stored in one core by the control winding during a period $T_s = 1/f_s$ are recovered through the gate winding during an interval T of the following period, during which interval the gate winding supports the clock voltage V_g, there is no drive to the inverting switching amplifier, and the power switch is closed. The interval T is determined by the volt-seconds stored and by the gate voltage V_g. At the end of the interval T the core saturates and the voltage V_g appears across the resistance R_g and is then applied to the inverting switching amplifier so that the power switch is opened for the remainder of the period T_s. The diodes and the square-wave clock voltage ensure that the cores perform these functions alternately and without interaction between the control and gate windings. The battery V_g is included as an analytical convenience to cancel the steering clock voltage, so that, for zero source resistance R_c, the voltage applied to the active control winding is V_c. Because of the push-pull nature of the modulator, the power switch repetition rate (the switching frequency f_s) is twice the frequency of the square-wave clock oscillator.

The subsystem may be classed as a buck power stage driven by a constant-frequency, or clocked, uniformly sampling integrating modulator: the control winding voltage is integrated over a period T_s, and is sampled uniformly at intervals T_s to determine the duty ratio $D \equiv T/T_s$ of the power switch drive for the following period T_s. Quantitatively, again for steady-state or d-c conditions and for zero source instance R_c, the volt-seconds Λ_0 stored by the control winding voltage V_c over a period T_s are $\Lambda_0 = V_c T_s$, and the same volt-seconds are then recovered under the gate voltage V_g to determine the following interval T, so that

$$D = \frac{T}{T_s} = \frac{V_c}{V_g} \qquad (3)$$

When the switch is closed, the voltage $v(t)$ at the filter input is equal to the line voltage V_ℓ, and if the conditions of operation of the power stage are constrained (as is usual) so that the inductor current never falls to zero, the diode clamps the voltage at the input of the filter to zero when the switch is open. It follows that the d-c component V of the switched voltage $v(t)$ at the filter input is simply equal to the time-average of V_ℓ and zero, namely

$$V = DV_\ell \qquad (4)$$

Since the d-c component of $v(t)$ is unaffected by the filter, the final result is

$$V_o = V = DV_\ell \qquad (5)$$

$$= \frac{V_\ell}{V_g} V_c \qquad (6)$$

Equation (6) represents the basic d-c operation of the modulator and power-stage subsystem, and contains both the control signal to output and line voltage to output transfer functions. For constant line voltage, the d-c output voltage is

proportional to the d-c control voltage, so the control to output transfer function is a constant. It may be seen that the possibility exists of making the line voltage to output transfer function zero: all that is required is to make V_g proportional to V_ℓ, which is easily achieved at least to first order approximation by making the amplitude of the clock oscillator output proportional to the line voltage.

Equation (6) also contains the two transfer functions with respect to incremental changes of sufficiently low frequency, that is, the two describing functions already introduced. Thus $F_c = V_\ell/V_g$ and $F_\ell = 0$ for sufficiently low frequency variations. However, because of the integration function of the modulator and the delay function inherent in the digital switch drive, at higher frequencies the output voltage ceases to follow the control signal and also cancellation of the line voltage variations ceases to be complete. The principal objective of the following analysis is the derivation of the two linearized describing functions $F_c(j\omega)$ and $F_\ell(j\omega)$ as functions of frequency, and to determine how these functions depend upon the resistance R_c of the control signal source and on appropriate parameters of the magnetic cores.

The problem of determination of the control signal to output voltage describing function can be formulated as follows. Let the line voltage be constant at V_ℓ, and let the control signal be a d-c plus a sinusoidal a-c voltage given by

$$v_c(t) = V_c + v_c \sin(\omega t - \theta) \tag{7}$$

where $t = 0$ is taken at the start of one of the switching periods T_s. This waveform is shown in Fig. 3(a). The duty ratio D_k for the kth period T_s is determined by the stored volt-seconds Λ_{k-1} at the beginning of that period. It will be shown that the "samples" Λ_{k-1} are points on a sine wave given by

$$\Lambda_{k-1} = \Lambda_0 + \lambda \sin[(k-1)(2\pi\omega/\omega_s) - \theta - \phi_m] \tag{8}$$

This sine wave and the uniform samples are shown in Fig. 3(b). The waveform $v(t)$ at the input to the filter is as shown in Fig. 3(c): it is a square wave of constant amplitude V_ℓ and constant repetition rate f_s, but of varying duty ratio. The interval T_k during which the power switch is closed is determined by the time taken to recover the stored volt-seconds Λ_{k-1} under the constant gate voltage V_g, so $T_k = \Lambda_{k-1}/V_g$ and the kth duty ratio D_k is

$$D_k = \frac{\Lambda_{k-1}}{V_g T_s} \tag{9}$$

Shown in Fig. 3(d) are the d-c component V and the component at the control frequency ω of the waveform $v(t)$. It will be shown that with neglect of all other components, the voltage at the filter input is given by

$$v(t) = V + v \sin(\omega t - \theta - \phi_m - \phi_d) \tag{10}$$

The component of the output voltage at the control frequency is merely the filter input voltage at that frequency modified by the filter characteristic, so that the control signal to output voltage describing function can be separated into two factors

$$F_c(j\omega) = F_c'(j\omega)\, F(j\omega) \tag{11}$$

where $F(j\omega)$ is the linear filter characteristic, and $F_c'(j\omega)$ is the describing function from the control signal to the filter input voltage. Henceforth, this describing function will be referred to as the control DF. From Eqs. (7) and (10), the control DF $F_c'(j\omega)$ is given by

$$F_c'(j\omega) = \frac{v}{v_c} e^{-j(\phi_m + \phi_d)} \tag{12}$$

It remains to determine the magnitude v/v_c and the phase lag $\phi_m + \phi_d$ of the control DF as functions of frequency and the various circuit parameters.

The problem of determination of the line voltage to output voltage describing function is formulated in a similar manner. Let the control signal be a constant voltage V_c, and let the line voltage be a d-c plus a sinusoidal a-c voltage given by

$$v_\ell(t) = V_\ell + v_\ell \sin(\omega t - \theta) \tag{13}$$

where $t = 0$ is again taken at the start of one of the switching periods T_s. This waveform is shown in Fig. 4(a). Also, let the gate voltage be proportional to the line voltage by a factor B, so that

$$v_g(t) = Bv_\ell(t) = B[V_\ell + v_\ell \sin(\omega t - \theta)] \tag{14}$$

and the desired complete cancellation in the output of d-c line variations is achieved. Since the control signal is constant, the stored volt-seconds at the sampling instants are constant at a value Λ_0, as shown in Fig. 4(b). The waveform $v(t)$ at the input to the filter is shown in Fig. 4(c): when the power switch is closed, $v(t)$ is equal to the line voltage $v_\ell(t)$. If the duty cycle were constant at a value D, $v(t)$ would contain a component of amplitude Dv_ℓ at the frequency ω; however, because the gate voltage is proportional to the line voltage, the constant stored volt-seconds Λ_0 are recovered over an interval T_k that varies with $v_g(t)$ and hence with $v_\ell(t)$, so that D_k is not constant but varies in such a way that the component of $v(t)$ at the frequency ω has an amplitude smaller than Dv_ℓ. It will be shown that, with neglect of all other sinusoidal components, the voltage at the filter input is given by

$$v(t) = V + v \sin(\omega t - \phi_\ell) \tag{15}$$

as shown in Fig. 4(d). Again, the line voltage to output voltage describing function can be separated into two factors

$$F_\ell(j\omega) = F_\ell'(j\omega)\, F(j\omega) \tag{16}$$

where $F_\ell'(j\omega)$ is the describing function from the line voltage to the filter input voltage.

Henceforth, this describing function will be referred to as the line DF. From Eqs. (13) and (15) the line DF $F'_\ell(j\omega)$ is given by

$$F'_\ell(j\omega) = \frac{v}{v_\ell} e^{-j\phi_\ell} \tag{17}$$

and it remains to determine the magnitude v/v_ℓ and the phase lag ϕ_ℓ of the line DF as functions of frequency and the various circuit parameters.

The procedure outlined above for determination of the control and line DF's will now be traced in detail.

3. THE CONTROL DESCRIBING FUNCTION

To obtain an analytical expression for the control DF, the first step is to find the stored volt-seconds Λ_{k-1} at the sampling instants $t = (k-1)T_s$. The case of zero source resistance $R_c = 0$ will be treated first, since it is particularly simple and affords a useful reference for the general case.

If $R_c = 0$, the control signal voltage $v_c(t) = V_c + v_c\sin(\omega t-\theta)$ is applied directly across the control winding. The core starts at, say, negative saturation, and the volt-seconds Λ_{k-1} stored during the period $(k-2)T_s < t < (k-1)T_s$ are given by

$$\Lambda_{k-1} = \int_{(k-2)T_s}^{(k-1)T_s} [V_c + v_c\sin(\omega t-\theta)]dt \tag{18}$$

The result is

$$\Lambda_{k-1} = V_c T_s + v_c T_s \frac{\sin(\pi\omega/\omega_s)}{(\pi\omega/\omega_s)} \sin[(k-1)(2\pi\omega/\omega_s) - \theta - (\pi\omega/\omega_s)] \tag{19}$$

which is of the form given in Eq. (8) in which

$$\Lambda_0 = V_c T_s \tag{20}$$

$$\lambda = v_c T_s \frac{\sin(\pi\omega/\omega_s)}{(\pi\omega/\omega_s)} \tag{21}$$

$$\phi_m = \pi\omega/\omega_s \tag{22}$$

It may be observed that the properties of the cores have not entered into this result, except that the B-H loop has been assumed sufficiently square that the qualitative operation is maintained.

In the general case where the control source resistance is not zero, the voltage applied across the control winding is less than the control voltage by the drop in R_c. Since this drop is dependent upon the current in the control winding, the properties of the core that relate current to voltage must now enter into the result. The model used to represent the properties of the cores is shown in Fig. 5. This is a B-H square-loop characteristic transformed to a Λ-I or volt-second--magnetizing current characteristic as seen by either the control or gate winding, which for simplicity are taken to have equal turns. Two principal second-order features are included in the model. First, the zero-flux magnetizing current I_m increases over its static value I_0 in proportion to the winding voltage $d\Lambda/dt$, or

$$I_m - I_0 = \frac{1}{R}\frac{d\Lambda}{dt} \tag{23}$$

where R has the nature of a resistance. This assumed linear relation between excess magnetizing current and voltage is an approximate representation of the well-known "loop widening effect". Second, the unsaturated part of the core characteristic is not vertical but represents a noninfinite inductance L. The two core-dependent quantities that affect the modulator properties are R and $\tau \equiv L/R$, where the resistance R is a function of the core material, geometry, and number of turns, and the time constant τ is a property of the core material only.

During any period T_s, the voltage across the control winding is $d\Lambda/dt$, and so the current through R_c is $I = [v_c(t) - d\Lambda/dt]/R_c$. This is also the total magnetizing current of the core $I = I_m + \Lambda/L$. Hence

$$v_c(t) - \frac{d\Lambda}{dt} = R_c\left(I_m + \frac{\Lambda}{L}\right) \tag{24}$$

After substitution for $v_c(t)$ and I_m, the differential equation for Λ is

$$\frac{d\Lambda}{dt} + r\frac{\Lambda}{\tau} = (1-r)V_c - rRI_0 + (1-r)v_c\sin(\omega t-\theta) \tag{25}$$

where

$$r \equiv \frac{R_c}{R+R_c} \tag{26}$$

The solution for $\Lambda(t)$ may be obtained and then, for the period T_s between $t=(k-2)T_s$ and $t=(k-1)T_s$, the volt-seconds stored are given by

$$\Lambda_{k-1} = \Lambda[t=(k-1)T_s] - \Lambda[t=(k-2)T_s] \tag{27}$$

where $\Lambda[t=(k-2)T_s] = -\Lambda_s$, the negative saturation value from which Λ starts at the beginning of each period T_s. It may be noted that if $R_c \to 0$, then $r \to 0$ and Eq. (25) reduces directly to Eq. (18) already obtained for the zero source resistance case.

After considerable algebraic manipulation, Λ_{k-1} obtained from Eqs. (25) and (27) may be expressed in the already mentioned form

$$\Lambda_{k-1} = \Lambda_0 + \lambda\sin[(k-1)(2\pi\omega/\omega_s) - \theta - \phi_m] \tag{28}$$

where

$$\Lambda_0 = \frac{1-e^{-\alpha}}{\alpha}[(1-r)V_c - rR(I_0 - \Lambda_s/L)]T_s \tag{29}$$

$$\lambda = \frac{1-e^{-\alpha}}{\alpha}(1-r)v_c T_s \sqrt{\frac{1+e^{-\alpha}\left(\frac{\alpha}{1-e^{-\alpha}}\right)^2\left(\frac{2}{\alpha}\right)^2 \sin^2\frac{\pi\omega}{\omega_s}}{1+\left(\frac{2}{\alpha}\right)^2\left(\frac{\pi\omega}{\omega_s}\right)^2}} \quad (30)$$

$$\phi_m = \tan^{-1}\left[\frac{\tan\left(\frac{\pi\omega}{\omega_s}\right)+(e^{\alpha}-1)\operatorname{cosec}\left(\frac{2\pi\omega}{\omega_s}\right)-\left(\frac{\alpha\omega_s}{\pi\omega}\right)}{1+\left(\frac{\alpha\omega_s}{\pi\omega}\right)\left[\tan\left(\frac{\pi\omega}{\omega_s}\right)+(e^{\alpha}-1)\operatorname{cosec}\left(\frac{2\pi\omega}{\omega_s}\right)\right]}\right] \quad (31)$$

in which

$$\alpha \equiv r\frac{T_s}{\tau} = \frac{R_c}{R+R_c}\frac{T_s}{\tau} \quad (32)$$

As a partial check, it may be seen that these rather formidable expressions reduce to those of Eqs. (20) through (22) for $R_c \to 0$. The complexity of these expressions occurs because in each period T_s the stored volt-seconds start from $-\Lambda_s$, and Λ_{k-1} is a transient solution of the differential equation Eq. (25). Also, neither the voltage nor current at the control winding is purely sinusoidal when $R_c \neq 0$, even though the control voltage is sinusoidal.

With Λ_{k-1} given by Eq. (28), D_k is given by Eq. (9) as

$$D_k = D + d\sin[(k-1)(2\pi\omega/\omega_s)-\theta-\phi_m] \quad (33)$$

where

$$D = \Lambda_0/V_g T_s \quad (34)$$

is the d-c duty ratio and

$$d = \lambda/V_g T_s \quad (35)$$

may be identified as the amplitude of the a-c duty ratio. Note that $0 < D < 1$, and $d < D$. With D given by Eq. (33), the complete waveform of the voltage $v(t)$ at the filter input, shown in Fig. 3(c), is known. It remains to find the d-c and fundamental a-c component at the frequency ω, shown in Fig. 3(d), which may be done by expressing $v(t)$ as a Fourier series. The actual procedure depends upon the nature of the relationship between the switching frequency f_s and the control frequency f. If

$$\frac{f}{f_s} = \frac{\omega}{\omega_s} = \frac{N}{M} = P \quad (36)$$

where N and M are positive integers, so that P is a rational number including zero and the integers, then f and f_s are said to be commensurate. It follows, with $T_s = 1/f_s$ and $T = 1/f$, that

$$MT_s = NT \quad (37)$$

or N periods of the control frequency contain M periods of the switching frequency. That is, the waveform $v(t)$ in Fig. 3(c) is repetitive with period $MT_s = NT$, and this is the shortest interval over which $v(t)$ can be integrated to obtain its Fourier series expansion. Figure 3 (and also Fig. 4) shows the waveform for the particular values $M = 10$, $N = 1$. If f and f_s are not commensurate, so that P is an irrational number, the waveform $v(t)$ is not periodic, and recourse must be taken to a double integration to obtain the Fourier components. Only the commensurate case will be treated here, since this is simpler and the results are the same as for the incommensurate case (1).

A convenient form for the Fourier series expansion of the voltage $v(t)$ at the filter input is

$$v(t) = K_0 + \sum_{n=1}^{\infty} |K_n|\sin(n\omega t + K_n) \quad (38)$$

where

$$K_0 = \frac{1}{2\pi N}\int_0^{2\pi N} v(t)\, d(\omega t) \quad (39)$$

$$K_n = \frac{j}{\pi N}\int_0^{2\pi N} v(t)\, e^{-jn\omega t}\, d(\omega t) \quad (40)$$

The integration interval $2\pi N$ covers N periods of f and M periods of f_s. Since only the d-c and the ω component of $v(t)$ are required, as shown in Fig. 3(d), only the $n = 1$ term in Eq. (38) is needed and the result can be expressed as

$$v(t) = V + v\sin(\omega t - \theta - \phi_m - \phi_d) \quad (41)$$

where

$$V = \frac{1}{2\pi N}\int_0^{2\pi N} v(t)\, d(\omega t) \quad (42)$$

$$v = |K_1| \quad (43)$$

$$\theta + \phi_m + \phi_d = -\angle K_1 \quad (44)$$

in which

$$K_1 = \frac{j}{\pi N}\int_0^{2\pi N} v(t)\, e^{-j\omega t}\, d(\omega t) \quad (45)$$

The form for $v(t)$ to be used in Eqs. (42) and (45) is that shown in Fig. 3(c), and expressed by

$$\left.\begin{aligned} v(t) &= V_\ell,\ (k-1)T_s < t < (k-1)T_s + T_k \\ v(t) &= 0,\ (k-1)T_s + T_k < t < kT_s \end{aligned}\right\} k = 1,2,\cdots M \quad (46)$$

Equation (42) then becomes

$$V = \frac{V_\ell}{2\pi N}\sum_{k=1}^{M}\int_{(k-1)\omega T_s}^{(k-1)\omega T_s+\omega T_k} d(\omega t) \quad (47)$$

which leads simply to the d-c value

$$V = DV_\ell \tag{48}$$

Equation (45) becomes

$$K_1 = \frac{jV_\ell}{\pi N} \sum_{k=1}^{M} \int_{(k-1)\omega T_s}^{(k-1)\omega T_s + \omega T_k} e^{-j\omega t}\, d(\omega t) \tag{49}$$

which, with $D_k = T_k/T_s$, leads to

$$K_1 = \frac{V_\ell}{\pi N} \sum_{k=1}^{M} \left[e^{-j\omega T_s(k-1)} - e^{-j\omega T_s(k-1+D)} e^{-j\omega T_s(D_k-D)} \right] \tag{50}$$

Consider the last exponential in Eq. (50). With D_k substituted from Eq. (33), this factor is

$$e^{-j\omega T_s(D_k-D)} = e^{-j2\pi(\omega/\omega_s)d \sin[(k-1)(2\pi N/\omega_s)-\theta-\phi_m]} \tag{51}$$

Since the amplitude v of the ω component in the filter input voltage $v(t)$ is proportional to K_1 and since the a-c duty ratio amplitude d is proportional to the amplitude v_c of the a-c control signal, Eq. (51) shows that v is a nonlinear function of v_c. Although the analysis can be continued in general [a Bessel function results (1)], a linearization restriction will be imposed here. The requirement is that the exponent of Eq. (51) should be sufficiently small that the exponential may be approximated by the first two terms of its series expansion:

$$e^{-j\omega T_s(D_k-D)} \simeq 1 - j[2\pi(\omega/\omega_s)d \sin[(k-1)(2\pi\omega/\omega_s)-\theta-\phi_m] \tag{52}$$

This makes v proportional to v_c, so that the control DF is linearized (independent of control signal a-c amplitude). The restriction required to validate the approximation of Fig. (52) is

$$2\pi(\omega/\omega_s)d << 1 \tag{53}$$

Since $d < D < 1$, this restriction is not very severe for control frequency ω less than the switching frequency ω_s. Further algebraic manipulation of Eq. (50), with the linearizing approximation of Eq. (52) included, eventually leads to

$$K_1 = \left[\frac{V_\ell}{(\pi\omega/\omega_s)} \left(1-e^{-j2D(\pi\omega/\omega_s)}\right) \right]_{\frac{\omega}{\omega_s}=1,2,3,\cdots} + \left[dV_\ell e^{-j[2D(\pi\omega/\omega_s)+\theta+\phi_m]} \right]_{\frac{\omega}{\omega_s}\neq\frac{1}{2},1,\frac{3}{2},\cdots}$$

$$+ \left[dV_\ell e^{-j[2D(\pi\omega/\omega_s)+\theta+\phi_m]} \left(1-e^{2j(\theta+\phi_m)}\right) \right]_{\frac{\omega}{\omega_s}=\frac{1}{2},1,\frac{3}{2},\cdots} \tag{54}$$

The significance of the contributions to this result is as follows. The term in the first square bracket is independent of d, so it exists in the absence of an a-c control signal; it represents the switching frequency and its harmonics. The term in the second square bracket is proportional to d, and represents the ω component that results directly from the a-c control signal. The term in the third square bracket, also proportional to d, represents the combination of the ω component that results directly from the a-c control signal and the appropriate sideband of the switching frequency. For example, for $\omega/\omega_s = 1/2$, the combination is of the direct component $\omega = (1/2)\omega_s$ and the sideband $\omega_s - \omega = (1/2)\omega_s$. It is seen that the amplitude of the ω component for $\omega/\omega_s = 1/2,1,3/2,\cdots$ can be as great as twice the amplitude for neighboring frequencies, the actual amplitude depending upon the phase θ of the control signal with respect to the switching frequency.

Since the components of K_1 for $\omega/\omega_s = 1,2,3,\cdots$ are present even in the absence of an a-c control signal, the term in the first square bracket in Eq. (54) is excluded from the DF representation. The remaining two terms may be combined into a single term in the following manner:

$$K_1 = dV_\ell\, e^{-j[2\pi(\pi\omega/\omega_s)+\theta+\phi_m]} \left(1-ke^{2j(\theta+\phi_m)}\right) \tag{55}$$

where $k = 1$ for the "special case" frequencies $\omega/\omega_s = 1/2,1,3/2,\cdots$, and $k = 0$ otherwise. The magnitude and phase of the ω component of the filter input voltage $v(t)$ are then obtained from Eqs. (43), (44), and (55) as

$$v = dV_\ell \left| 1-ke^{2j(\theta+\phi_m)} \right| \tag{56}$$

$$\phi_d = 2D(\pi\omega/\omega_s) - \angle\left(1-ke^{2j(\theta+\phi_m)}\right) \tag{57}$$

The results may now be assembled as follows. The d-c control transfer function is obtained from Eqs. (48), (34), and (29) as

$$V = \frac{V_\ell}{V_g} \left(\frac{1-e^{-\alpha}}{\alpha}\right) [(1-r)V_c - rR(I_0 - \Lambda_s/L)] \tag{58}$$

where

$$r = \frac{R_c}{R+R_c} \tag{59}$$

$$\alpha = \frac{T_s}{\tau} = \frac{R_c}{R+R_c}\frac{T_s}{\tau} \tag{60}$$

It is convenient to normalize the a-c control DF

$F'_c(j\omega)$ to its zero-frequency value $F'_c(j0)$, and to define the resulting normalized control signal to filter input voltage DF as H'_c, which is obtained from Eq. (12) with insertion of Eqs. (56), (57), (35), and (30) as

$$H'_c \equiv \frac{F'_c(j\omega)}{F'_c(j0)} = A\, e^{-j[2D(\pi\omega/\omega_s)+\phi_m]} \left(\frac{2j(\theta+\phi_m)}{1-ke} \right)$$

where

$$F'_c(j0) = \frac{V_\ell}{V_g} \frac{1-e^{-\alpha}}{\alpha} \frac{R}{R+R_c} \tag{62}$$

and

$$A \equiv \sqrt{\frac{1 + e^{-\alpha}\left(\frac{\alpha}{1-e^{-\alpha}}\right)^2 \left(\frac{2}{\alpha}\right)^2 \sin^2 \frac{\pi\omega}{\omega_s}}{1 + \left(\frac{2}{\alpha}\right)^2 \left(\frac{\pi\omega}{\omega_s}\right)^2}} \tag{63}$$

$$\phi_m = \tan^{-1}\left[\frac{\tan\left(\frac{\pi\omega}{\omega_s}\right) + (e^{\alpha}-1)\operatorname{cosec}\left(\frac{2\pi\omega}{\omega_s}\right) - \left(\frac{\alpha\omega_2}{\pi\omega}\right)}{1+\left(\frac{\alpha\omega_s}{\pi\omega}\right)\left[\tan\left(\frac{\pi\omega}{\omega_s}\right) + (e^{\alpha}-1)\operatorname{cosec}\left(\frac{2\pi\omega}{\omega_s}\right)\right]} \right] \tag{64}$$

with

$$k = \begin{cases} 0\ , & \omega/\omega_s \neq 1/2,1,3/2,\cdots \\ 1\ , & \omega/\omega_s = 1/2,1,3/2,\cdots \end{cases} \tag{65}$$

Equation (61) shows that a polar plot of the a-c control DF H'_c is a trajectory traced out by a phasor of length A and angle $-[2D(\pi\omega/\omega_s)+\phi_m]$, but that at the special-case frequencies $\omega/\omega_s = 1/2,1,3/2,\cdots(k=1)$ the total phasor is the sum of the first phasor with $k=0$ and a second phasor of equal magnitude but with an angle that depends upon the phase θ of the control a-c signal with respect to the switching frequency. The second phasor describes a circle, centered on the end of the first phasor, as $\theta+\phi_m$ varies from 0 to π. A qualitative sketch of such a polar plot of H'_c is shown in Fig. 6. At the frequencies $\omega/\omega_s = 1/2,1,3/2,\cdots$ the total phasor has an amplitude that varies from zero to 2A, and a phase angle that varies up to $\pm\pi/2$ from $-[2D(\pi\omega/\omega_s)+\phi_m]$, depending upon θ.

Separate magnitude and phase plots of the a-c control DF H'_c vs. frequency are shown in Figs. 7 and 8, with α as a parameter. From Eq. (61),

$$|H'_c|[\omega/\omega_s \neq 1/2,1,3/2,\cdots] = A \tag{66}$$

$$\angle H'_c[\omega/\omega_s \neq 1/2,1,3/2,\cdots] = -[2D(\pi\omega/\omega_s)+\phi_m] \tag{67}$$

$$|H'_c|[\omega/\omega_s = 1/2,1,3/2,\cdots] = 2A\sin(\theta+\phi_m) \tag{68}$$

$$\angle H'_c[\omega/\omega_s = 1/2,1,3/2,\cdots] = -[2D(\pi\omega/\omega_s)+\phi_m] - [(\theta+\phi_m)-\pi/2] \tag{69}$$

For $\alpha = 0$, that is, for voltage-driven control signal with $R_c = 0$, the magnitude and phase factors A and ϕ_m due to the magnetic modulator reduce to

$$A = \frac{\sin(\pi\omega/\omega_s)}{(\pi\omega/\omega_s)} \tag{70}$$

$$\phi_m = \pi\omega/\omega_s \tag{71}$$

In Fig. 7, magnitude plots are given for $\alpha = 0$, 1.5, and 10. The frequency dependence stems entirely from the modulator. In Fig. 8, phase plots are given for $\alpha = 0$ and 1.5, with the d-c duty ratio $D = 0.5$. The total phase lag is made up of the two components shown, $2D(\pi\omega/\omega_s)$ due to the power stage, and ϕ_m due to the modulator.

The zero to double-amplitude possibility expressed by Eq. (68) is represented in Fig. 7 by "spikes" superimposed upon the amplitude A at the special-case frequencies $\omega/\omega_s = 1/2,1,3/2,\cdots$. The spike extends 6 db above and ∞ db below the corresponding amplitude A. To avoid cluttering the picture, only a few of these spikes are shown in Fig. 7, but they are present at $\omega/\omega_s = 1/2,1,3/2,\cdots$ for all values of α. The $\pm\pi/2$ additional phase lag expressed by Eq. (69) is similarly represented in Fig. 8 by $\pm\pi/2$ spikes superimposed upon the phase lag $[2D(\pi\omega/\omega_s)+\phi_m]$ at the special-case frequencies $\omega/\omega_s = 1/2,1,3/2,\cdots$. [The $\pm\pi/2$ range is given by Eq. (69) for $0 < \theta+\phi_m < \pi$; for $\pi < (\theta+\phi_m) < 2\pi$, the additional lag π is cancelled by the sign reversal of the amplitude factor given by Eq. (68).] Again, only a few of the spikes are shown in Fig. 8.

The most important feature of the results displayed in the control signal DF plots of Figs. 7 and 8 is that the performance of the modulator and power stage subsystem is improved if the modulator is driven from a current source rather than from a voltage source. The performance is improved in the sense that the frequency response of the control DF is extended: the magnitude decay and the phase lag at a given frequency are both less for $\alpha > 0$ than for $\alpha = 0$. Extended frequency response translates directly into improved gain and phase margins when the subsystem is inside a feedback loop. The improvement is quite substantial: at $\omega/\omega_s = 0.8$, for example, the phase lag for $\alpha = 1.5$ is less by about $\pi/2$ than that for $\alpha = 0$, but the magnitude increase is only about 3.5 db. The degree of improvement in the frequency response is, however, limited by the maximum value of α given by Eq. (60) with $R_c \to \infty$ for a current-source control signal:

$$\alpha_{max} = \frac{T_s}{\tau} \tag{72}$$

3.1 Experimental Results

Experimental results for the control signal DF H'_c were obtained on a circuit embodying the principle illustrated in Fig. 2. Each core was a Magnetics Inc. 51056-2H, Type 48 Alloy. The

control and gate windings each consisted of 500 turns of No. 26 wire. The clock square-wave was obtained from an Exact 301 Function Generator at 1 kHz, so the switching frequency was $f_s = 2$ kHz with $T_s = 0.5$ msec. The peak value of the gate square wave was $V_g = 14$ v. Since the modulated square-wave voltage $v(t)$ at the filter input is the same as that at the modulator output (except for a scale factor and phase reversal) the power stage was omitted, and replaced by a Schmitt trigger to sharpen the modulator output waveform, which is soft because of the soft saturation characteristic of the cores. The control d-c and a-c signals were obtained from a low output impedance amplifier, either directly for voltage drive $V_c (R_c=0)$, or via a common-emitter transistor stage for current drive $I_c = V_c/R_c$ $(R_c=\infty)$. A Hewlett-Packard 302A Wave Analyzer was used to measure the magnitude of the control-signal frequency component in the Schmitt trigger modulated square-wave output waveform $v(t)$. In the BFO mode, the wave analyzer provides a signal at the frequency to which the voltmeter is tuned, so this signal was used to supply the control signal a-c component.

The experimental results for $|H_c'|$ obtained in this way are shown in Fig. 9. The solid line is the theoretical result for $\alpha = 0$ taken from Fig. 7 and it is seen that the corresponding experimental points for voltage drive ($R_c=0$, $\alpha=0$) agree quite closely with the theoretical curve. The experimental points for current drive ($R_c=\infty, \alpha=\alpha_{max}$) also lie on a curve of the expected shape, and are well fitted by the theoretical curve for $\alpha = 0.95$. Hence from Eq. (72),

$$\tau = \frac{T_s}{\alpha_{max}} = \frac{0.5}{0.95} = 0.53 \text{ msec} \qquad (73)$$

To verify the presence of the "spikes" in the $|H_c'|$ plot, the a-c control signal must be synchronized with the switching frequency. In the experimental set-up described, this can be done very simply for $\omega/\omega_s = 1/2$ by use of the sine-wave output of the Exact Function Generator, which is available simultaneously with the square-wave output at the same frequency used for the clock, which is $\omega_s/2$. The sine-wave output at $\omega = \omega_s/2$ was applied as the a-c control signal through a phase-shifting network, and the amplitude of the control signal was adjusted, for each value of phase angle, to the (constant) value previously used for the measurements at other frequencies. Measurements were made for voltage drive, and are shown in Fig. 10. The results agree well with the theoretical curve, also shown, expressed by Eq. (68) with A and ϕ_m given by Eqs. (70) and (71) for $\omega/\omega_s = 1/2$:

$$|H_c'|[\omega/\omega_s=1/2] = \frac{2}{\pi/2} \sin(\theta + \pi/2) \qquad (74)$$

The measurements shown in Figs. 9 and 10 were all taken at a d-c duty ratio $D = 0.9$. Since the 302A Wave Analyzer makes only magnitude measurements, experimental verification of the theoretical phase relations of Fig. 8 was not obtained. However, the agreement between the theoretical and the experimental magnitude relations is sufficiently good to inspire confidence in the theoretical expression for the control signal DF.

Experimental measurements were also made of the d-c control transfer characteristic. From Eqs. (34) and (29), the theoretical relation between the d-c duty ratio D and the control signal is

$$D = \frac{1}{V_g} \frac{1-e^{-\alpha}}{\alpha} [(1-r)V_c - rR(I_0 - \Lambda_s/L)] \qquad (75)$$

For voltage drive V_c with $R_c=0$, $r=0$ and $\alpha=0$, so

$$D\Big|_{\alpha=0} = \frac{V_c}{V_g} \qquad (76)$$

For current drive $I_c = V_c/R_c$ with $R_c=\infty$, $r=1$ and $\alpha=\alpha_m$, so

$$D\Big|_{\alpha=\alpha_m} = \frac{1-e^{-\alpha_m}}{\alpha_m} \frac{R}{V_g}[I_c - \Lambda_s/L)] \qquad (77)$$

Experimental measurements of $D|_{\alpha=0}$ vs. V_c and $D|_{\alpha=\alpha_m}$ vs. I_c are shown in Figs. 11 and 12. The duty ratio was determined by direct observation of the Schmitt trigger output waveform $v(t)$ on an oscilloscope. The $D|_{\alpha=0}$ transfer characteristic is linear over essentially the entire range $0 < D < 1$, but the $D|_{\alpha=\alpha_m}$ characteristic becomes nonlinear at both ends of the range. This is because the actual cores do not have the sharp saturation characteristic assumed in the model of Fig. 5. However, a substantial part of the range is linear with a slope of 1/0.54 ma. The measured slope of the $D|_{\alpha=0}$ characteristic is 1/12 v and from Eqs. (76) and (77) the value of R can be obtained from

$$\frac{1-e^{-\alpha_m}}{\alpha_m} R = \frac{12 \text{ v}}{0.54 \text{ ma}} = 22.2\text{k} \qquad (78)$$

With the previously determined value $\alpha_m = 0.95$, the result is $R = 34$k.

As described above, the performance of the cores in the modulator permits experimental determination of the core second-order parameters R and τ. However, the first-order core parameters Λ_s and I_0 can also be obtained. An independent measurement showed that the total volt-seconds supportable by the core with 500 turns was $2\Lambda_s = 3.9$ v-msec, so that $\Lambda_s = 1.95$ v-msec. This converts to $B_s = 9.1$ kgauss, compared with the manufacturer's nominal value of 11.6 kgauss. The value of I_0 can be obtained from the intercept of the $D|_{\alpha=\alpha_m}$ characteristic with the current axis, from Fig. 12 and Eq. (77) as

$$I_0 - \Lambda_s/L = 0.72 \text{ ma} \qquad (79)$$

The nonsaturated inductance $L = R = 0.53$ msec $\times$ 34k = 18h, so $\Lambda_s/L = 1.95/18 = 0.11$ ma and

$I_0 = 0.72 + 0.11 = 0.83$ ma. This converts to $H_0 = 0.12$ oersted, compared with the manufacturer's nominal value of 0.1 oersted.

It may be observed that the measured slope of the $D|_{\alpha=0}$ characteristic in Fig. 11, 1/12 v, does not agree with the value $1/V_g$ predicted by Eq. (76) when $V_g = 14$ v. This is because the voltage that actually appears across the gate winding is less than V_g by a diode drop of about 0.6 v, and by the drop in the load resistance R_g due to the core magnetizing current. Although the magnetizing current changes during the interval T_s that the core is resetting (because of the finite inductance L), an approximate average value is $I_m = I_0 + (1/R)d\Lambda/dt$. If the gate winding voltage is assumed to be the measured value $d\Lambda/dt = 12$ v, $I_m = 0.83 + 12/34 = 1.18$ ma. The value of R_g used in the experimental set-up was $R_g = 1.35$k, so the effective gate winding voltage is $14-0.6-(1.18\times1.35) = 14-0.6-1.6 = 11.8$ v, in satisfactory agreement with the observed 12 v. This effective value of V_g should, of course, also be employed in the $D|_{\alpha=\alpha_m}$ characteristic of Eq. (77). The discrepancy in the offset of the $D|_{\alpha=0}$ characteristic observed in Fig. 11 occurs because the effective control winding voltage is less than V_c by a diode drop of about 0.6 v.

4. THE LINE DESCRIBING FUNCTION

As for the control DF, the analytic derivation of the line DF is in two parts. In the first part an expression for the kth duty ratio D_k is obtained, and in the second part the coefficient K_1 of the ω component in the filter input voltage waveform $v(t)$ is obtained by Fourier analysis.

A qualitative description of the signal conditions has been given in Section 2 with reference to Fig. 4. The line voltage has a d-c plus a sinusoidal component given by Eq. (13), and the gate voltage is proportional to the line voltage as in Eq. (14). The control signal is constant at Λ_0. These volt-seconds are recovered under the action of the gate voltage $v_g(t)$ to determine T_k by

$$\int_{(k-1)T_s}^{(k-1)T_s+T_k} v_g(t)\,dt = \Lambda_0 \tag{80}$$

The duty ratio D_k is then given by

$$B\int_{(k-1)}^{(k-1)+D_k} [V + v\sin(\omega t-\theta)]d(t/T_s) = \Lambda_0 = DBV_\ell \tag{81}$$

where the second equality is obtained by recognition that $D_k = D$, the d-c duty ratio, when $v_\ell = 0$. Evaluation of the integral in Eq. (81) leads to a transcendental relation for D_k. However, a closed-form solution can be obtained as

$$D_k = D + d\sin[(k-1)(2\pi\omega/\omega_s)-\theta+D\pi\omega/\omega_s] \tag{82}$$

where

$$d \equiv -D\frac{\sin(D\pi\omega/\omega_s)}{(D\pi\omega/\omega_s)} \times \frac{v_\ell/V_\ell}{1+(v_\ell/V_\ell)\sin[(k-1)(2\pi\omega/\omega_s)-\theta+D\pi\omega/\omega_s]} \tag{83}$$

under the restriction

$$2\pi(\omega/\omega_s)d \ll 1 \tag{84}$$

Equation (82) corresponds to Eq. (33) obtained for control signal variations. Also, the restriction of Eq. (84) is the same as that required in the control signal analysis, Eq. (53). It may be noted that the restriction does not involve v_ℓ/V_ℓ, and so Eq. (82) is valid even for large fractional line voltage variations. However, d is independent of k, and so the D_k points lie on a sine wave, only if $v_\ell/V_\ell \ll 1$.

The expression for the Fourier coefficient K_1 of the ω component in the filter input waveform $v(t)$ is established in the same way as for control signal variation in Eqs. (38) through (49), the only difference being that $v(t) = V_\ell + v_\ell\sin(\omega t-\theta)$ instead of V_ℓ during the switch on-times T_k. Hence, for line variations, the equation for K_1 corresponding to Eq. (49) is

$$K_1 = \omega T_s\frac{jV_\ell}{\pi N} \times \sum_{k=1}^{M}\int_{(k-1)}^{(k-1)+D_k}[1+(v_\ell/V_\ell)\sin(\omega t-\theta)]e^{-j\omega t}d(t/T_s) \tag{85}$$

Again, commensurate frequencies are assumed such that $\omega/\omega_s = N/M$ where N and M are integers. Evaluation of the integral subject to the restriction of Eq. (84) permits K_1 to be expressed as a linear function of D_k, which can then be substituted by Eq. (82). Evaluation of the k summations then leads to three groups of terms, as in the control variations case. The harmonics of the switching frequency, present even in the absence of line variations, are irrelevant, and the sideband combinations can be neglected since it is unlikely that line variations synchronous with the switching frequency would exist. The remaining term that results directly from the a-c line component is

$$K_1 = Dv_\ell e^{j\theta}\left(1 - \frac{1-e^{-j2D(\pi\omega/\omega_s)}}{j2D(\pi\omega/\omega_s)}\right) \tag{86}$$

The a-c line DF is then $F'_\ell(j\omega) = K_1/(v_\ell e^{-j\theta})$, and it is convenient to normalize $F'_\ell(j\omega)$ to its infinite-frequency value $F'(j\infty)$, and to define

the resulting normalized line to filter input voltage DF as H'_ℓ, which is

$$H'_\ell \equiv \frac{F'_\ell(j\omega)}{F'_\ell(j\infty)} = 1 - \frac{1-e^{-j2D(\pi\omega/\omega_s)}}{j2D(\pi\omega/\omega_s)} \tag{87}$$

where

$$F'_\ell(j\infty) = D \tag{88}$$

The magnitude and phase of the a-c line DF H'_ℓ are given by

$$|H'_\ell| = \sqrt{\left(1 - \frac{\sin(2D\pi\omega/\omega_s)}{2D\pi\omega/\omega_s}\right)^2 + \left(\frac{\sin^2(D\pi\omega/\omega_s)}{D\pi\omega/\omega_s}\right)^2} \tag{89}$$

$$\underline{H'_\ell} = \tan^{-1}\left[\frac{2\sin^2(D\pi\omega/\omega_s)}{(2D\pi\omega/\omega_s) - \sin(2D\pi\omega/\omega_s)}\right] \tag{90}$$

Since the d-c duty ratio D always appears as a multiplier of ω, a single plot of $|H'_\ell|$ may be made as a function of $2D\omega/\omega_s$, as shown in Fig. 13. As anticipated, $|H'_\ell|$ is zero at zero frequency when the line change applied to the power switch is exactly compensated by the change of duty ratio resulting from the corresponding change in gate voltage. However, as the frequency of the line variations increases, the increasing phase delay through the modulator prevents complete compensation; ultimately, for frequencies such that $2D\omega/\omega_s$ is greater than about 2π, there is essentially no compensation and the line variations appear unmodified in the filter input voltage. Since in a practical application the phase $\underline{/H'_\ell}$ is of little concern, a plot of $\underline{/H'_\ell}$ is not given; however, it can be seen from Eq. (90) that $\underline{/H'_\ell} = \pi/2$ at zero frequency, and ultimately for high frequencies decreases to zero.

For frequencies sufficiently low that $(2D\omega/\omega_s) << 2/\pi$, Eqs. (89) and (90) reduce to

$$|H'_\ell| = \frac{\pi}{2}\,\frac{2D\omega}{\omega_s} \tag{91}$$

$$\underline{/H'_\ell} = \frac{\pi}{2} - \tan^{-1}\left(\frac{\pi}{3}\,\frac{2D\omega}{\omega_s}\right) \tag{92}$$

5. CONCLUSIONS

A particular pulse-width modulator and power switch subsystem that has been widely used in practical switching-mode d-c regulators has been analyzed. The subsystem may be classed as a buck power stage driven by a clocked uniformly sampling integrating modulator employing square-loop cores, whose principle of operation is illustrated in Fig. 2.

The analysis leads to an expression for the describing function $F'_c(j\omega)$ that relates a sinusoidal control signal at frequency ω at the modulator input to the resulting source frequency component of the filter input voltage. The overall describing function from the control signal to the output voltage is then $F_c(j\omega) = F'_c(j\omega)\,F(j\omega)$, where $F(j\omega)$ is the filter linear transfer function. When the control input is voltage driven (zero source resistance) normal operation is independent of core parameters and the normalized control DF $H'_c \equiv F'_c(j\omega)/F'_c(j0)$ is of the form $\sin(\pi\omega/\omega_s)/(\pi\omega/\omega_s)$. However, the frequency response is extended when the control signal is driven from a nonzero resistance source as expressed by Eq. (61) and shown in Figs. 7 and 8. Extension of the frequency response is quantitatively related to two second-order core parameters, the "loop widening" resistance R and the nonsaturated inductance L. The theoretical results are confirmed in Fig. 9 by experimental measurements made on a practical circuit. The complete knowledge of the control DF thus obtained is valuable in optimizing the design of feedback regulators in which this particular subsystem is used.

Analysis is also presented that leads to an expression for the describing function $F'_\ell(j\omega)$ that relates a sinusoidal line voltage variation at frequency ω to the resulting source-frequency component of the filter input voltage. The overall describing function from the line voltage to the output voltage is then $F_\ell(j\omega) = F'_\ell(j\omega)/F(j\omega)$. When the modulator gate voltage is made proportional to the line voltage, the normalized line DF $H'_\ell \equiv F'_\ell(j\omega)/F'(j\infty)$ is zero for zero-frequency variations but increases with frequency, as shown by Eq. (87) and in Fig. 13. Thus, even though complete cancellation of line variations can be obtained at zero-frequency, line "feedthrough" occurs at higher frequencies, and the analytical results derived here can be used to determine the overall line sensitivity of the output voltage in a complete feedback regulator system.

REFERENCE

(1) G. W. Wester and R. D. Middlebrook, "Low-Frequency Characterization of Switched DC-DC Converters", Third IEEE Power Processing and Electronics Specialists Conference, Atlantic City, May 1972.

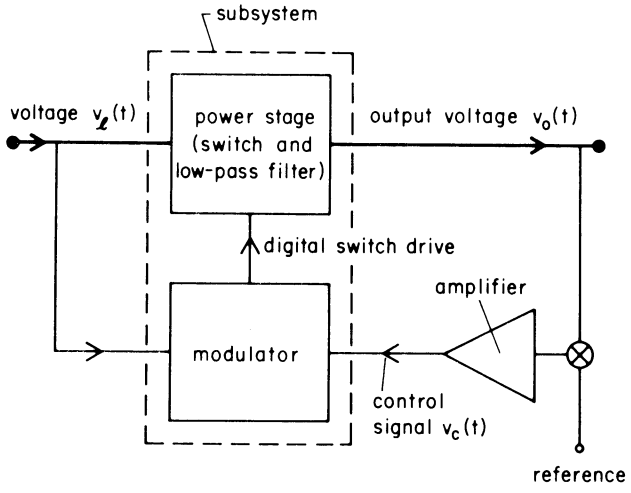

Fig. 1 Block diagram of typical closed-loop d-c regulator including a subsystem containing a modulator and switched power stage.

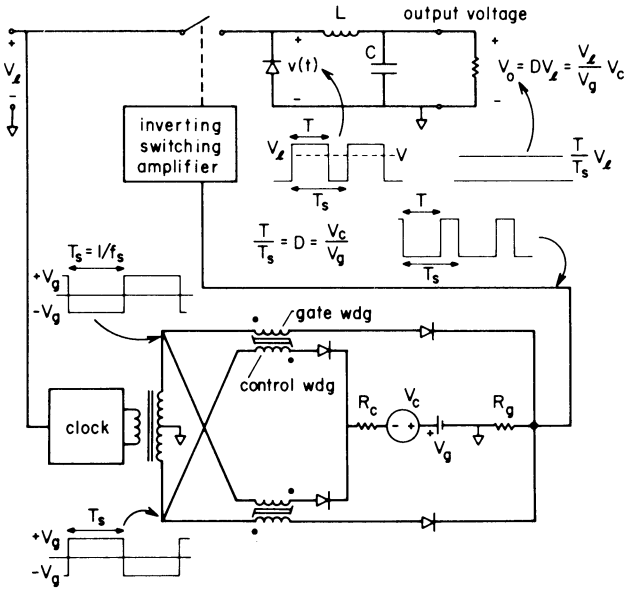

Fig. 2 A specific subsystem consisting of a power switch and filter in buck configuration and a constant-frequency variable duty-ratio push-pull magnetic modulator employing square-loop cores.

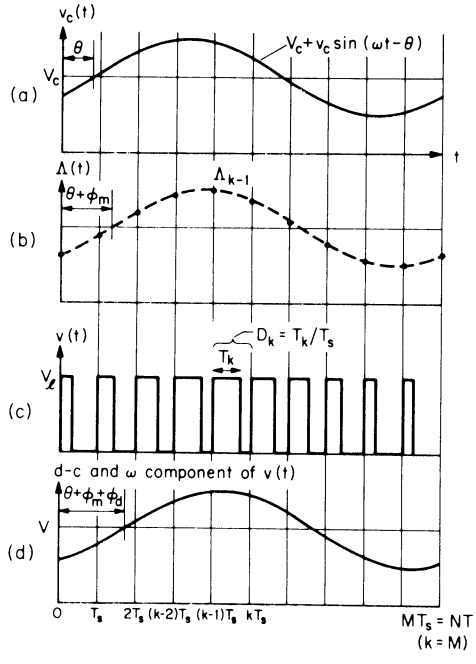

Fig. 3 Waveforms in the subsystem of Fig. 2 for d-c plus sinusoidal control signal.

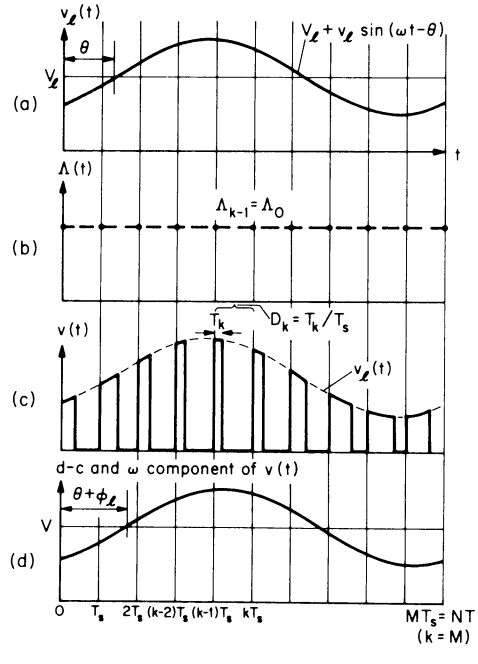

Fig. 4 Waveforms in the subsystem of Fig. 2 for d-c plus sinusoidal line voltage.

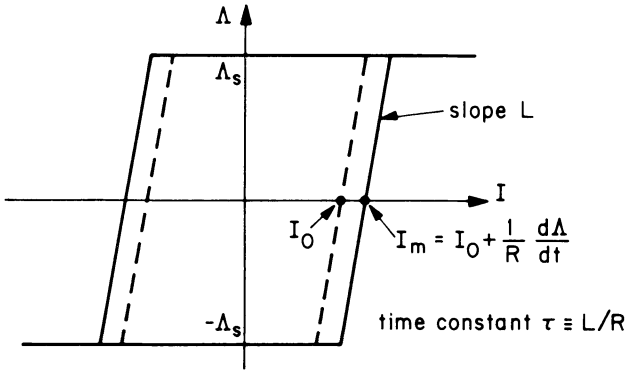

Fig. 5 Core model including two second-order parameters, the loop-widening resistance R and the noninfinite unsaturated inductance L.

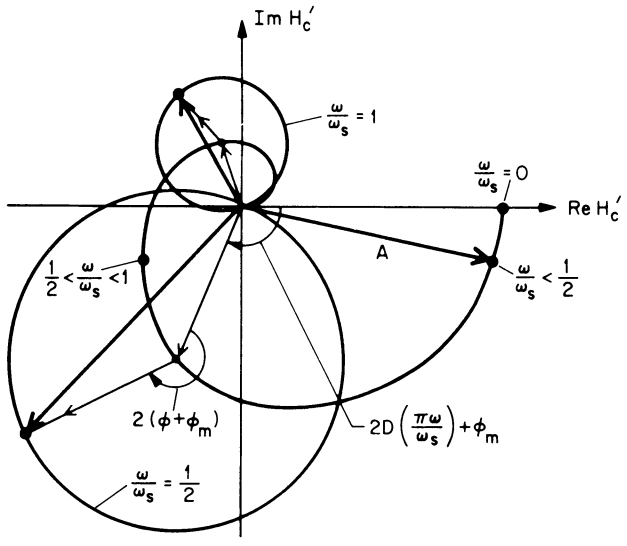

Fig. 6 Polar plot of the normalized control DF H_c', showing the two phasor components at $\omega/\omega_s = 1/2, 1, 3/2, \cdots$, and the single phasor component at other frequencies.

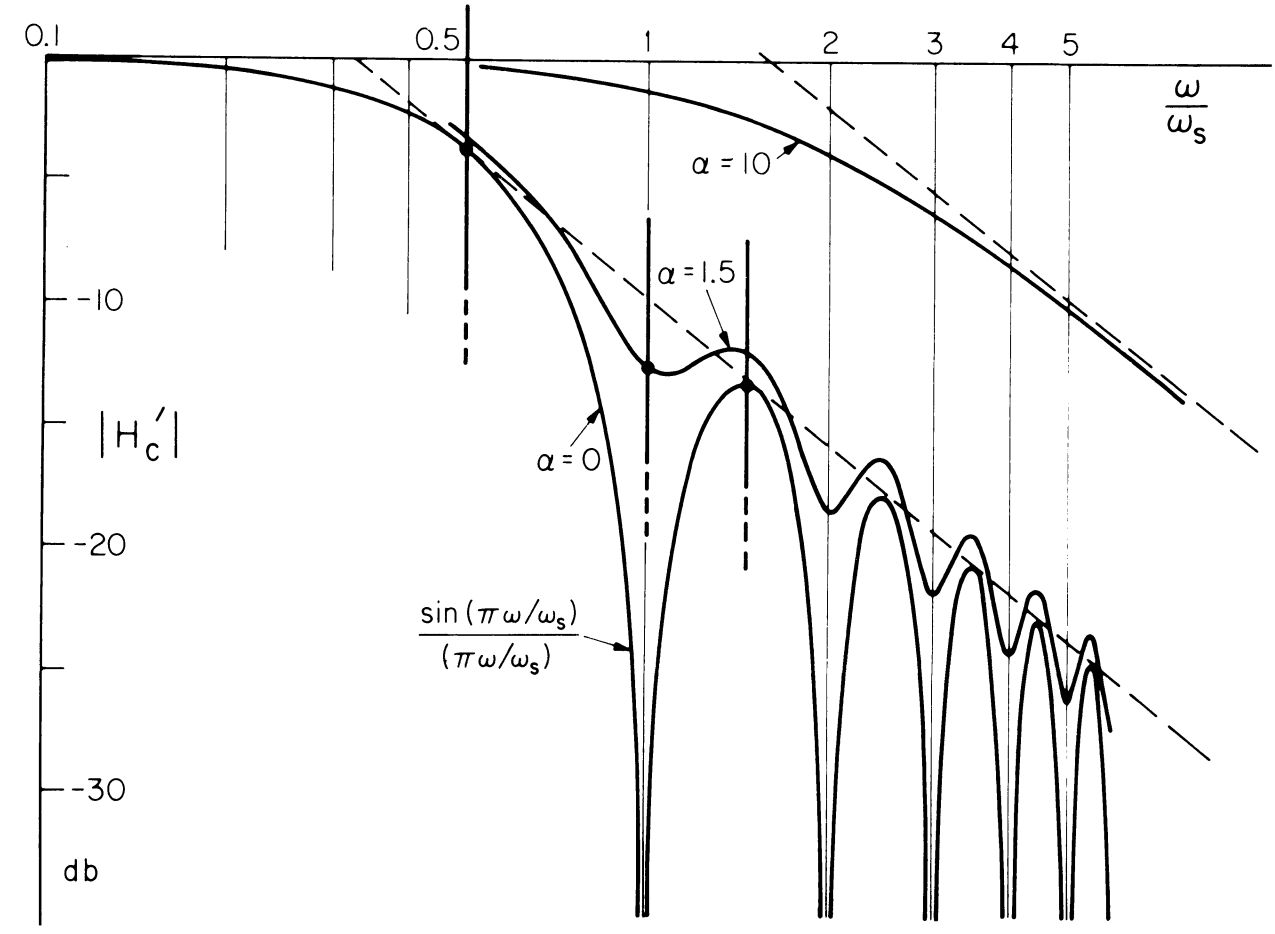

Fig. 7 Theoretical magnitude vs. frequency plot of the control DF H_c', for $\alpha = 0$, 1.5, and 10, showing the "spikes" at $\omega/\omega_c = 1/2, 1, 3/2, \cdots$.

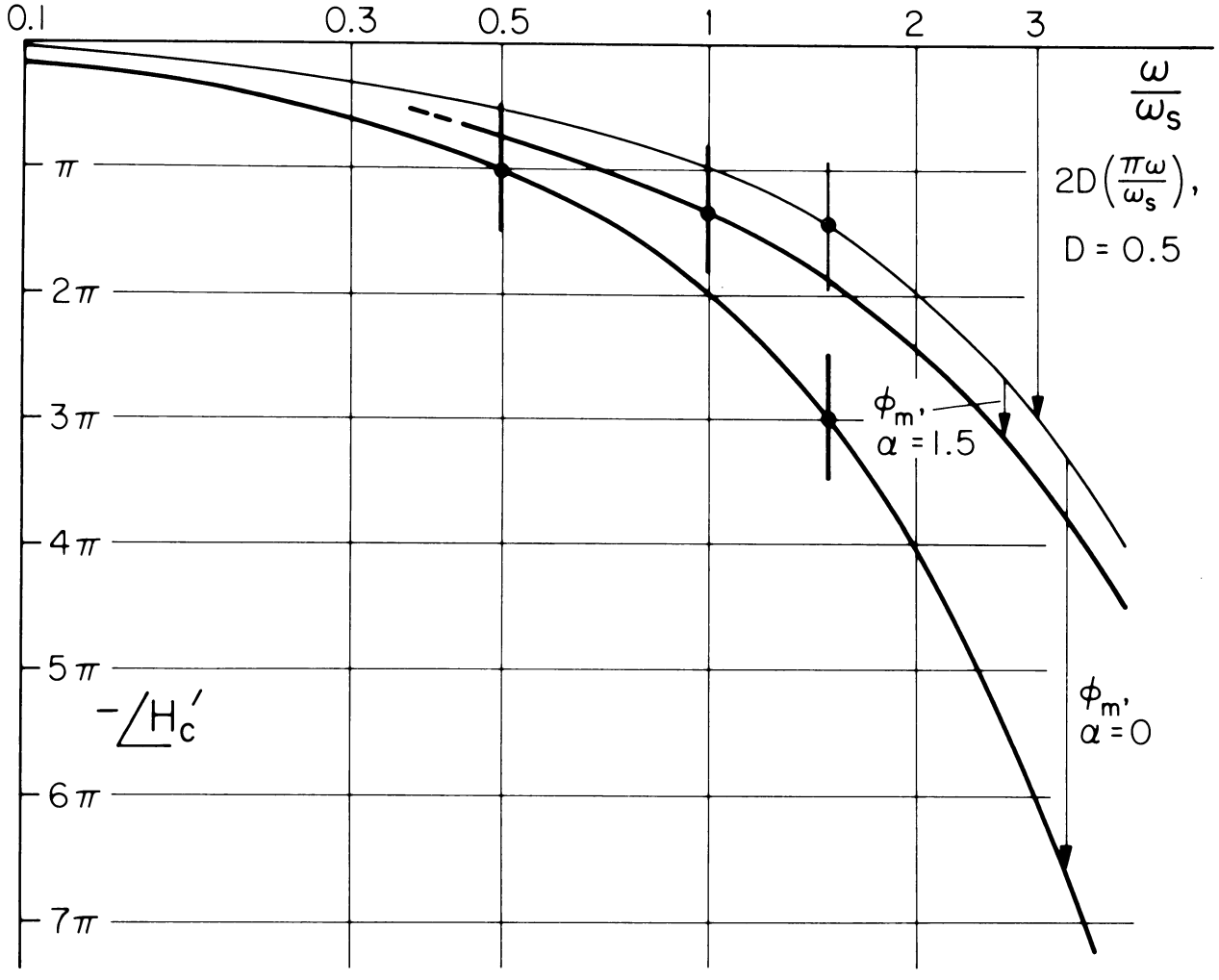

Fig. 8 Theoretical phase vs. frequency plot of the control DF H_c', showing the component $2D(\pi\omega/\omega_s)$ from the power stage for $D = 0.5$, and the component ϕ_m from the modulator for $\alpha = 0$ and 1.5.

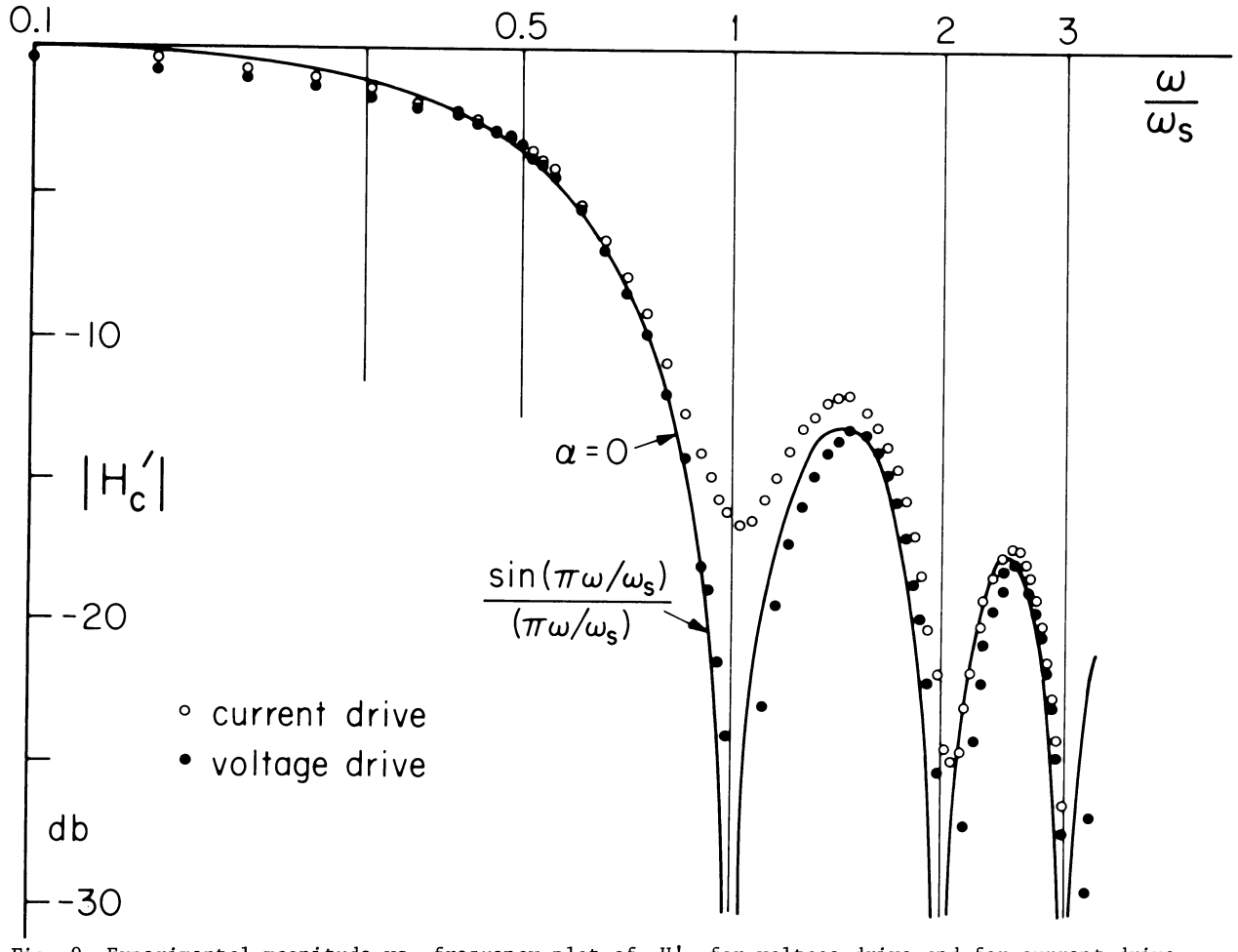

Fig. 9 Experimental magnitude vs. frequency plot of H_c' for voltage drive and for current drive.

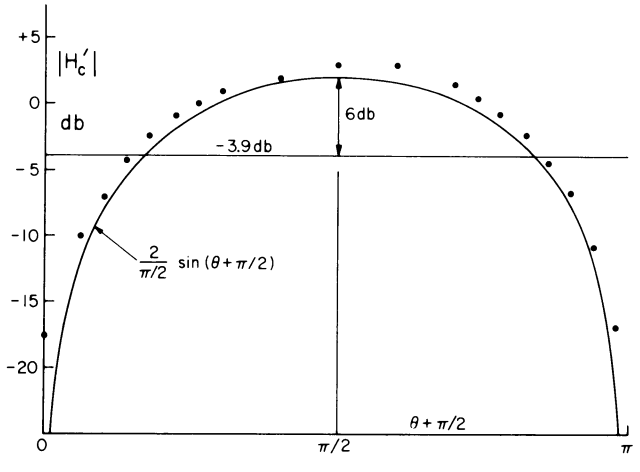

Fig. 10 Theoretical and experimental magnitude of H_c' vs. the phase θ of the control signal, for $\omega/\omega_s = 1/2$.

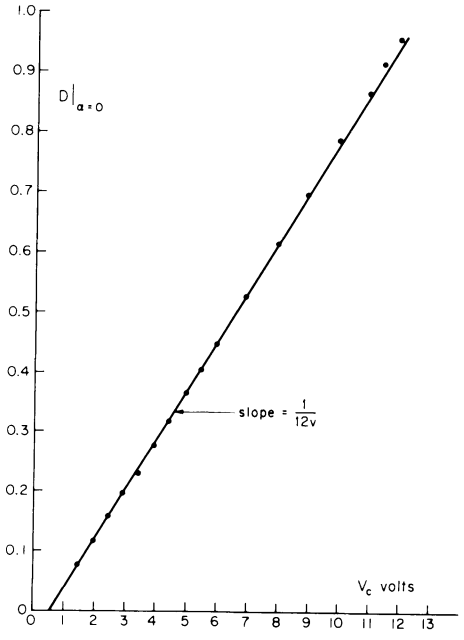

Fig. 11 Duty ratio D vs. control voltage V_c, for voltage drive ($\alpha = 0$).

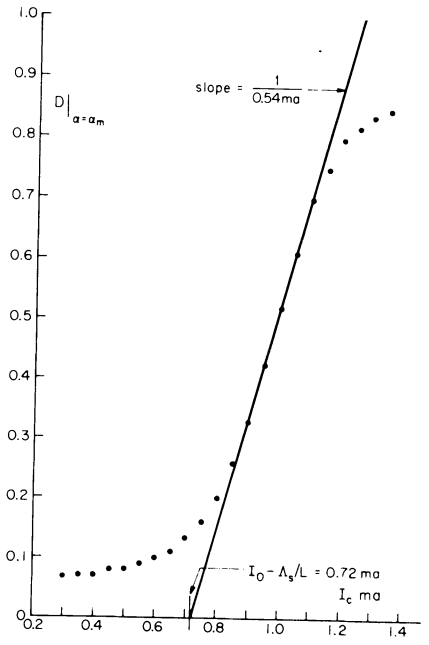

Fig. 12 Duty ratio D vs. control current I_c, for current drive ($\alpha = \alpha_m$).

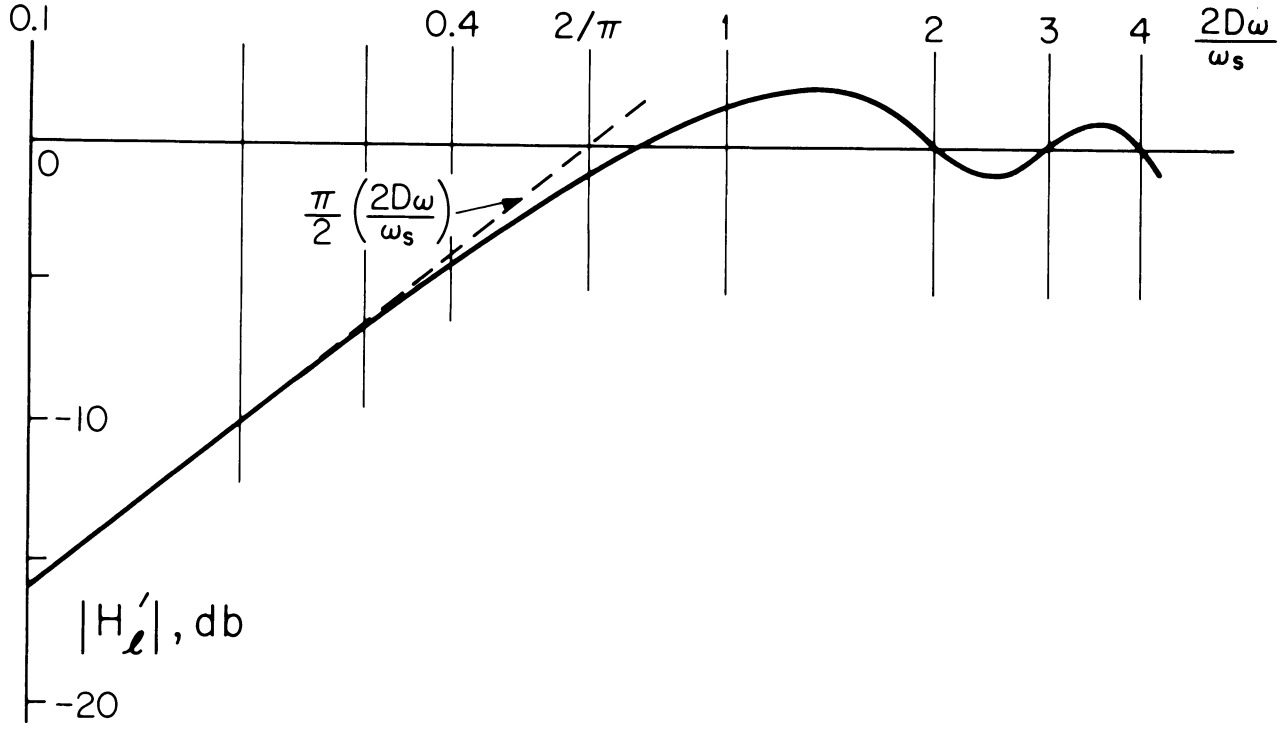

Fig. 13 Theoretical magnitude vs. frequency plot of the line DF H'_ℓ.